ARTICLES

Initial Excited-State Structural Dynamics of Thymine Are Coincident with the Expected Photochemical Dynamics

Soujanya Yarasi, Philip Brost, and Glen R. Loppnow*

Department of Chemistry, University of Alberta, Edmonton, Alberta, T6G 2G2, Canada

Received: February 20, 2007; In Final Form: April 10, 2007

To explore the excited-state structural dynamics of thymine, a DNA nucleobase, we measured the resonance Raman spectra of thymine in aqueous solution at wavelengths throughout the lowest-energy absorption band. Self-consistent analysis of the resulting resonance Raman excitation profiles and absorption spectrum using a time-dependent wave packet formalism yielded the excited-state structural dynamics. The photochemically relevant C═C stretching and C−H deformation vibrational modes were found to exhibit maximum resonance Raman intensity and structural change upon photoexcitation for thymine, suggesting that the initial dynamics of thymine lie along the photochemical reaction coordinate.

Introduction

Deoxyribonucleic acid (DNA), which stores genetic information, and ribonucleic acid (RNA), which mediates translation of the genetic code into proteins, are composed of two purines, adenine and guanine, and three pyrimidines, cytosine, thymine, and uracil.[1] Thymine (Scheme 1) is found only in DNA. It is well-known that upon UV irradiation, thymine dinucleotides preferentially form the cyclobutyl photodimer (CPD) with a quantum yield, ϕ, of 0.013 as a result of [2 + 2]-cycloaddition between the C═C bonds of adjacent thymines or the [6 − 4]-photoproduct ($\phi = 0.003$) as a result of [2 + 2]-cycloaddition between the C═C bond of one thymine and the C═O bond of the adjacent thymine.[2,3] Earlier investigations[4] have shown that molecular oxygen and isoprene, two triplet quenchers, do not have any effects on the quantum yield of photodimers and photohydrates, suggesting that the photochemistry arises from the singlet state. Moreover, $\phi_{isc} = 10^{-4}$ for thymine is much lower than $\phi_{photoproducts}$.

An argument used to justify the evolution of these nucleobases in modern DNA is their rapid excited-state relaxation, resulting in efficient dissipation of energy. Femtosecond UV multiphoton ionization has measured gas-phase excited-state lifetimes of thymine of 6.4 ps.[5] Time resolved absorption and fluorescence show much shorter lifetimes of 0.3−0.7 and 0.5−1 ps for aqueous thymidine and thymidine monophosphate, respectively.[6−8] However, these rates represent electronic relaxation only, with little information about molecular structural changes occurring in the photochemically active excited state.

A number of computational studies has been performed on the photochemical reaction coordinate of thymine.[9−13] B3LYP DFT[11,12] and CASSCF/cc-pVDZ[9] ab initio calculations predict an excited-state photochemical reaction coordinate for thymine that is quite flat at the Franck−Condon region, has a small barrier followed by a well at the transition state, and then rises sharply toward the photodimer minimum. Also, B3LYP DFT calculations predict a transition-state structure in noncovalently associated thymine dimers where the two rings are puckered and the C_5 and C_6 carbons are more pyramidalized.[12] Resonance Raman spectroscopy is a uniquely appropriate method for testing the validity of these predictions, particularly near the Franck−Condon region.

SCHEME 1

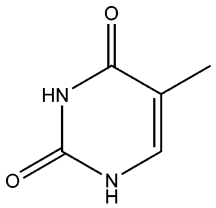

Thymine

Resonance Raman vibrational scattering spectroscopy is a powerful probe of excited-state molecular structure and initial dynamics.[14] By tuning the exciting laser into an absorption band, resonant enhancement of those normal vibrational modes coupled to the electronic excitation occurs. A resonance Raman vibrational band intensity is directly proportional to the slope of the excited-state potential energy surface along that vibrational coordinate; the greater the change in molecular structure in the electronic excited-state along a particular nuclear coordinate, the greater the resulting resonance Raman intensity in that vibrational band.[14] Thus, the resonance Raman intensities directly reflect the conformational distortion of the molecule along each normal mode upon excitation to an electronic excited state.

Resonance Raman studies of several deoxyribonucleotides and ribonucleotides at different excitation wavelengths have been previously performed.[15−17] There has been only one attempt to quantify the observed changes in the excited states

* To whom correspondence should be addressed. E-mail: glen.loppnow@ualberta.ca.

10.1021/jp071443t CCC: $37.00
Published on Web 05/27/2007

of these species. Peticolas and co-workers[18−20] used the Kramers−Kronig transform technique to estimate the amount of geometry change on excitation for uracil and thymine. However, the experimental and calculated resonance Raman spectra did not agree. Specifically, the 1235 cm^{-1} band of uracil was underestimated and the 1662 cm^{-1} band of thymine was overestimated with this procedure.[20] No systematic quantitative analysis of the excited-state dynamics of thymine have been performed to date. This early work, while substantial for its time, suffered from an incomplete understanding of the vibrations of the nucleobases and a lack of quantitative measurement of the excited-state structural dynamics. It is fundamentally important to understand the structural and photochemical behavior of simple molecules like nucleobases to understand the photochemistry of complex molecules like DNA and RNA.

In this paper, the initial excited-state dynamics of thymine were determined from its UV resonance Raman spectra excited within the intense, longest-wavelength absorption band centered at 260 nm. The results show the ability of resonance Raman spectroscopy to distinguish the important structural and environmental determinants of excited-state dynamics. The observed excited-state structural dynamics of thymine, which ultimately lead to nonradiative de-excitation, are coincident with those expected for the photochemical products. In other words, these excited-state relaxational modes are localized at the site of photochemical reactivity. The experimental excited-state structural dynamics measured here are compared to those predicted from computational studies of thymine excited states and photoreactivity.

Experimental Procedures

Thymine (5-methyl-2,4-dioxopyrimidine, 99%, Sigma, Oakville, Ontario) and sodium sulfate (99%, Merck KgaA, Darmstadt, Germany) were obtained commercially and used as supplied. Nanopure water from a Barnstead water filtration system (Boston, MA) was used to prepare the thymine solutions. Sodium sulfate was used as an internal intensity standard and did not have a noticeable affect on either the absorption or resonance Raman spectra of thymine. Typical concentrations of thymine were 3−5 mM and of sulfate were 0.4−0.5 M.

Resonance Raman scattering was excited by spherically focusing the laser onto an open stream of flowing solution in a 135° backscattering geometry. Laser excitation was obtained with an Ar^+ pumped or doubled Nd:YVO_3 pumped, picosecond mode-locked Ti:sapphire laser and harmonic generator (Coherent, Santa Clara, CA). Wavelengths of 233, 250, 257, 266, 275, and 290 nm were obtained by doubling the Ti:sapphire fundamental in a lithium triborate (LBO) crystal followed by third-harmonic generation in a β-barium borate (β-BBO) crystal. Typical laser powers were 5−20 mW. The laser system and spectrometer have been described in detail previously.[21] Frequency calibration was performed by measuring Raman scattering of solvents of known frequencies (acetonitrile, dimethylformamide, carbon tetrachloride, ethanol, and pentane). Frequencies are accurate to ±2 cm^{-1}. Absorption spectra were recorded on a diode array spectrophotometer (Hewlett-Packard, model 8452A, Sunnyvale, CA). Measurement of the resonance Raman spectra and determination of the intensities were repeated on three fresh samples of thymine at each wavelength. Analysis of the data was performed as previously described.[14] Bleaching of the sample was corrected by averaging the measured solution absorbance before and after each scan. The observed bleaching in a 60 min scan was <5%, suggesting that the bulk photoalteration parameter is small.[22−25] Similarly, the low photochemistry quantum yield of ~0.02 suggests a negligible single-pass photoalteration parameter.[24]

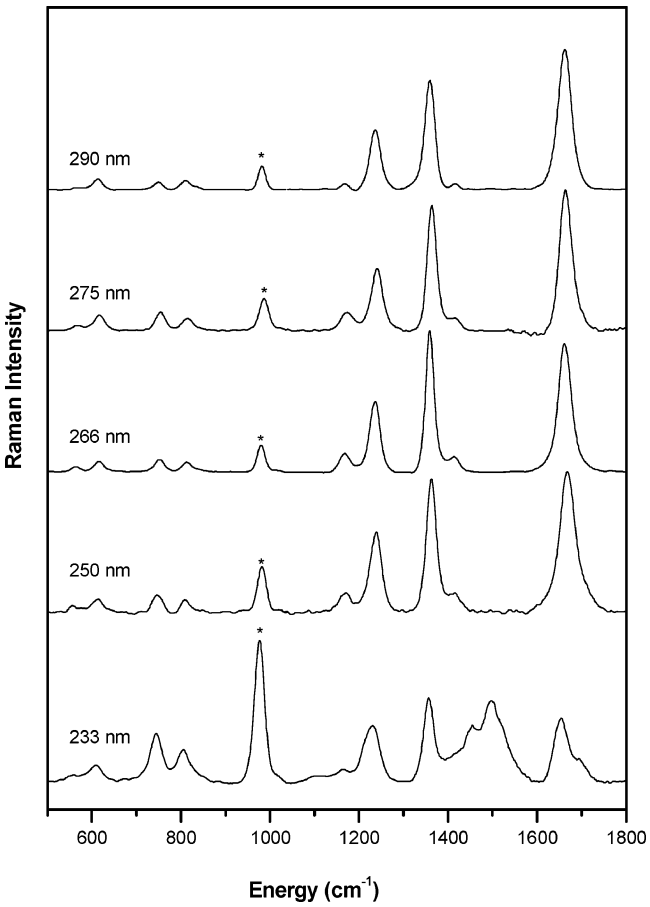

Figure 1. UV resonance Raman spectra of 3 mM thymine in water at excitation wavelengths within the 260 nm absorption band. The spectra are the sum of three to nine scans. The ca. 0.4 M sulfate internal standard Raman peak is indicated by an asterisk.

The resonance Raman spectrum of thymine in the overtone and combination band region was recorded with a UV Raman microscope (Renishaw, Chicago, IL). Resonance Raman scattering was excited by focusing the UV laser beam at 257 nm onto a drop of thymine or uracil (6−7 mM) in an aqueous solution containing 0.4−0.5 M sulfate in a 180° backscattering geometry. Frequencies were calibrated against the 1332 cm^{-1} vibration of diamond. Measurement of the resonance Raman spectra and determination of the intensities were repeated on three fresh samples of thymine. Analysis of the data was performed as previously described.[14]

The methods used here for converting the resonance Raman intensities of thymine into absolute cross-sections and for self-absorption correction effects have been described previously.[21−25] The experimental sulfate cross-sections used were 4.0×10^{-11}, 2.7×10^{-11}, 2.28×10^{-11}, 2.0×10^{-11}, 1.7×10^{-11}, and 1.3×10^{-11} $Å^2$/molecule at 233, 250, 257, 266, 275, and 290 nm, respectively.

Theory

The resonance Raman excitation profiles were simulated with the time-dependent wavepacket propagation formalism[14,26]

$$\sigma_R(E_L) = \frac{8\pi E_S^3 E_L e^4 M^4}{9\hbar^6 c^4}\int_0^\infty dE_0 H(E_0)\left|\int_0^\infty dt\langle f|i(t)\rangle \exp\left\{\frac{i(E_L+\epsilon_i)t}{\hbar}\right\}G(t)\right|^2 \quad (1)$$

$$\sigma_A(E_L) = \frac{4\pi E_L e^2 M^2}{6\hbar^2 cn}\int_0^\infty dE_0 H(E_0)\int_{-\infty}^\infty dt\langle i|i(t)\rangle \exp\left\{\frac{i(E_L+\epsilon_i)t}{\hbar}\right\}G(t) \quad (2)$$

where E_L and E_S are the energies of the incident and scattered photons, respectively, n is the refractive index, M is the transition length, ϵ_i is the energy of the initial vibrational state, $|i\rangle$ and $|f\rangle$ are the initial and final vibrational wavefunctions in the Raman process, $H(E_0) = (2\pi\theta)^{-1/2}\exp\{-(\bar{E}_0 - E_0)^2/2\theta^2\}$ is a normalized inhomogeneous distribution of zero−zero energies around an average energy, $\bar{E}_0$, $|i(t)\rangle = e^{-iHt/\hbar}|i\rangle$ is the initial ground-state vibrational wavefunction propagated on the excited-state potential surface, and $G(t)$ is the homogeneous line width function. For molecules interacting with a bath, $G(t)$ represents the dynamics of chromophore−solvent coupling. Significantly, the $\langle i|i(t)\rangle$ and $\langle f|i(t)\rangle$ overlaps are only sensitive to Δ, the difference in ground- and excited-state equilibrium geometries along each normal mode, within the separable harmonic oscillator approximation. Thus, the resonance Raman intensities directly reflect the structural dynamics of the excited state.

The Brownian oscillator model developed by Mukamel[27] is used here to model the solute−solvent interactions that contribute to the solvent-induced homogeneous broadening. The general implementation of these equations for absorption and resonance Raman spectroscopy has been previously described in detail.[28] This model treats the solvent response as arising from one or more linearly coupled vibrational modes each characterized by a frequency, and a coupling strength. In the analysis presented here, the strongly overdamped and high-temperature ($\hbar\Lambda \ll kT$) limits have been used.

For this analysis, the initial guesses for the displacements along each normal coordinate (Δ) were found from the relative resonance Raman vibrational intensities excited at 266 nm assuming that the intensities were proportional to Δ^2 and with the intensity of the 1662 cm^{-1} mode set arbitrarily to 1. The relative Δ values were scaled to give the experimentally observed absorption and resonance Raman excitation profile bandwidths. All nine observed fundamental vibrational modes in thymine were used in the time-dependent calculations. The overtone vibrations below 3000 cm^{-1} of thymine were used to further constrain the simulation. Other parameters were selected to give the best calculated absorption spectrum and resonance Raman excitation profiles. The parameters were then optimized iteratively as described previously[29] until the calculated and experimental absorption spectrum and resonance Raman excitation profiles were in agreement.

Results

The UV resonance Raman spectra of thymine are shown in Figure 1. Nine bands for thymine are observed between 500 and 1700 cm^{-1} and have been previously assigned[30,31] (Table 1). The assignments listed here are from the most recent DFT computation[30] and appear to be consistent with the largest set of isotopomers ever measured for thymine,[30,31] although they differ somewhat from previous assignments of thymine vibrations. Weaker bands in the 500−800 cm^{-1} region are clearer in Figure 1 than in previously reported spectra,[32−34] as a result of the better spectral signal-to-noise ratios here. Apart from excitation at 233 nm, there are no frequency shifts or relative intensity changes as the Raman excitation wavelength is scanned through the absorption band, indicating that the Raman spectra are enhanced by a single electronic transition. At 233 nm, the relative intensities observed in the resonance Raman spectra change, suggesting that resonance enhancement of the vibrations by the ca. 200 nm absorption band is occurring. Thymine exhibits three main, intense bands, a $C-CH_3$/ring stretch at 1237 cm^{-1}, a coupled C_6H bend/$C_5{=}C_6$ stretch at 1359 cm^{-1}, and a primarily $C_5{=}C_6$ stretch at 1662 cm^{-1}.

Quantitative measurement of the resonance Raman cross-section of each fundamental vibration as a function of excitation wavelength within the absorption band yields the resonance Raman excitation profiles. Figure 2 shows the experimental and simulated absorption spectra of thymine, while Figure 3 shows the experimental and simulated resonance Raman excitation profiles (RREPs) of thymine modeled with eqs 1 and 2 and the parameters in Table 1. Figures 2 and 3 illustrate the good agreement between experimental and calculated resonance Raman excitation profiles and absorption spectra. Deviations in the simulated absorption spectrum at energies greater than 42 000 cm^{-1} are due to higher electronic transitions, which were not modeled (vide infra). The different relative Raman intensities of vibrational bands seen in Figure 1 are directly reflected in the different experimental Raman cross-sections (Figure 3) and excited-state geometry displacements (Table 1).

To better constrain the parameter set that accurately describes the absorption spectra and fundamental resonance Raman excitation profiles, the overtones and combination bands between 1700 and 3000 cm^{-1} were also measured at 257 nm. Although some overtones are expected at frequencies greater than 3000 cm^{-1}, these were obscured by the broad O−H stretching vibrations of water. It is well-known that the overtone and combination band intensities are much more sensitive to the excited-state geometry displacements (Δ) and provide an additional constraint on the excited-state parameters. The experimental and calculated cross-sections for all of the observed overtones and combination bands of thymine are given in Table 2.

Self-consistent analysis of the absorption and resonance Raman excitation profiles with eqs 1 and 2 permits the partitioning of the spectral breadth into inhomogeneous and homogeneous components. These two factors affect the observed absorption and resonance Raman excitation profile differently. The inhomogeneous component arises from ensemble site effects and only broadens the absorption spectrum and resonance Raman excitation profiles, while the homogeneous line width represents contributions from excited-state population decay and pure dephasing, which dampens out the resonance Raman scattering intensity and broadens both. As one can see from Table 1, both homogeneous and inhomogeneous line widths used need to be fairly large to reproduce both the absolute Raman intensities and the absorption band shape.

Discussion

Photochemistry. The primary photoproducts of thymine, the cyclobutyl photodimer and the [6 − 4]-pyrimidine pyrimidinone, both involve a change in the bond order of the C_5C_6 bond from a double bond to a single bond. Therefore, if the initial excited-state structural dynamics lie along the photochemical reaction coordinate, it is reasonable to expect that excited-state distortions should involve a lengthening of the C_5C_6 bond and greater pyramidalization of C_5 and C_6 as the hybridization changes from

TABLE 1: Harmonic Mode Parameters of Thymine[a]

mode (cm^{-1})	mode assignment[b]	$\|\Delta\|$
563	$90\gamma(N_1H_7) - 6\gamma(N_3H_9)$	0.12
616	$28be(C_4O_{10}) - 27be(C_2O_8) + 14be(C_5C_{11}) + 6$ring def 2	0.17
752	$60\gamma(C_2O_8) - 12$ring def $6 + 8$ring def $4 + 6\gamma(C_4O_{10}) - 5\gamma(N_3H_9)$	0.2
813	45ring def $1 + 20\nu(C_5C_{11}) - 11\nu(N_1C_2)$	0.17
1168	$21\nu(C_2N_3) + 20be(C_6H_{12}) - 16be(N_1H_7) - 12\nu(N_3C_4) - 11\nu(C_6N_1)$	0.34
1237	$29\nu(C_5C_{11}) - 21\nu(C_6N_1) - 12$ring def $1 + 10\nu(N_1C_2) - 10\nu(C_4C_5) - 8\nu(C_2N_3)$	0.66
1359	$42be(C_6H_{12}) + 12\nu(C_5C_6) + 9\nu(N_1C_2) - 9\nu(C_2N_3)$	0.81
1412	$15\nu(C_2N_3) - 13\nu(C_4C_5) - 11CH_3$ umb $+ 9be(N_1H_7) - 8\nu(N_1C_2) + 7be(C_4O_{10}) + 7be(C_2O_8) -$ 6ring def $2 - 6be(N_3H_9)$	0.35
1662	$61\nu(C_5C_6) - 13be(C_6H_{12}) - 8\nu(C_6N_1) - 5\nu(C_5C_{11})$	0.84

[a] Frequencies listed are the experimental frequencies reported here. Displacements (Δ) are in units of dimensionless normal coordinates and were obtained by fitting eqs 1 and 2 with the following parameters: $T = 0$ K, Brownian oscillator lineshape $\kappa = \Lambda/D = 0.1$, Gaussian homogeneous line width $\Gamma_G = 355$ cm^{-1}, inhomogeneous line width $\Theta = 1200$ cm^{-1}, $E_0 = 36\,525$ cm^{-1}, and transition length $M = 0.735$ Å. The estimated errors in the parameters used in the calculation are as follows: zero−zero energy (E_0) ±1%, transition length (M) ±1%, homogeneous line width (Γ) ±5%, inhomogeneous line width (Θ) ±5%, and displacements ±5%. [b] Mode assignments from ref 35. Abbreviations: ν, stretching; def, deformation; γ, wagging; umb, umbrella; and be, bending. Numbers represent the total percentage potential energy distribution (PED) of the listed internal coordinate(s) to the normal mode. Only PEDs greater than 5% have been listed. Positive and negative PEDs represent the phases of the respective internal coordinate contributions.

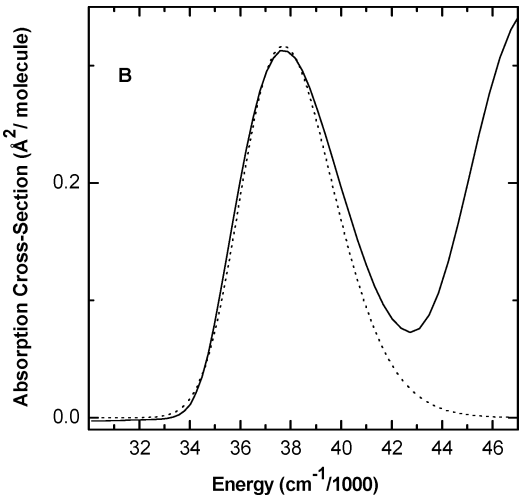

Figure 2. Experimental (solid line) and simulated (dotted line) absorption spectra of thymine. Simulated absorption spectra were calculated by using eq 2 with the parameters of Table 1. Discrepancies at energies greater than 42 000 cm^{-1} are due to higher energy electronic transitions that were not modeled here.

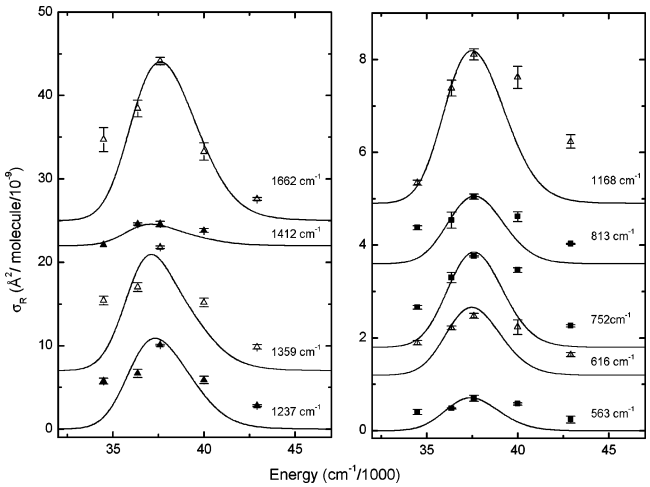

Figure 3. Experimental (points) and calculated (solid line) resonance Raman excitation profiles of thymine. Excitation profiles were calculated with eq 1 by using the parameters of Table 1. Excitation profiles have been offset along the ordinate for greater clarity of presentation.

sp^2 to sp^3. These structural dynamics are exactly those reflected in the predicted transition-state structure,[12] but it is not clear as to whether these occur early or late on the excited-state potential energy surface. Since the resonance Raman intensities are proportional to the excited-state slope (i.e., the classical force) along each vibrational normal mode, an analysis of the resonance Raman intensities can distinguish between these two models of the excited-state structural dynamics in thymine. Indeed, from the UV-induced photochemical products of thymine, one can predict which vibrational bands in a resonance Raman spectrum will have intensity, if the initial excited-state structural dynamics lie along the photochemical reaction coordinate. For thymine, the formation of either the cyclobutyl photodimer or the [6 − 4]-photodimer results in lengthening of the $C_5{=}C_6$ bond due to the change from double bond to more single bond character. Therefore, we would expect intensity in the $C_5{=}C_6$ stretching mode in the resonance Raman spectrum for thymine. Similarly, because of the hybridization change from sp^2 carbons to sp^3 carbons at C_5 and C_6, one can expect intensity in the $C_6{-}H$ and $C_5{-}CH_3$ bending, deformation, and wagging modes.

The major conclusion of this work is that the resonance Raman spectra demonstrate that the derived excited-state structural dynamics for thymine lie coincidentally with the photochemical reaction coordinate (i.e., the structural dynamics that yield the photochemical products occur early on the excited-state potential energy surface near the Franck−Condon region). Table 1 shows that the structural dynamics for thymine lays primarily along the 1662, 1359, and 1237 cm^{-1} modes, respectively, since these have the largest Δs. The projection of these excited-state displacements on the photochemical reaction coordinate depends on accurate descriptions of the vibrational modes.[35] For thymine, these vibrations at 1237, 1359, and 1662 cm^{-1} are assigned to a $C_5{-}Me$ + ring stretch, a $C_6{-}H$ bend + $C_5{=}C_6$ stretch, and the $C_5{=}C_6$ stretch, respectively (Table 1), all vibrations localized near the photochemical reaction site and expected to exhibit significant resonance Raman intensity. The resonance Raman spectrum of thymine (Figure 1) corresponds well with our predictions; the $C_5{=}C_6$ stretching and $C_6{-}H$

TABLE 2: Experimental and Calculated Absolute Resonance Raman Overtone and Combination Band Cross-Sections for Thymine[a]

mode (cm^{-1})	σ_{exptl} (Å²/molecule × 10^{-9})	σ_{calcd} (Å²/molecule × 10^{-9})
2596	3.06 ± 0.12	4.66
2720	3.03 ± 0.10	3.64
2899	4.35 ± 0.98	2.91
3014	5.68 ± 0.90	5.19

[a] Excitation wavelength is 257 nm. Cross-sections were calculated with eq 1 by using the parameters of Table 1.

deformation modes are the most intense bands in the resonance Raman spectrum and have the largest excited-state geometry changes.

Another way to quantify these results is to borrow the idea of reorganization energies from electron transfer theory.[36,37] The reorganization energy along each vibrational normal mode can be calculated from $E = \nu\Delta^2/2$, where E is the reorganization energy of a particular mode in cm^{-1}, ν is the wavenumber of that vibration, and Δ is the excited-state equilibrium geometry displacement in dimensionless normal coordinates. Using this equation, 87% of the excited-state reorganization energy is in the 1237, 1359, and 1662 cm^{-1} modes, while only 13% is in the more dissipative modes, again reinforcing the conclusion that most of the initial excited-state structural dynamics are directed along the photochemical reaction coordinate.

These results on thymine provide support for the DFT prediction of the transition state of the UV photoinduced [2 +2]-cycloaddition reaction of thymine.[12] These calculations predict a transition state for the photodimerization of thymine with a puckered geometry where the C_5-C_6 bond has been lengthened the most of all bonds, from 1.35 to 1.49 Å. The bond length change (δR) for thymine from the ground-state equilibrium geometry to the transition-state geometry can be calculated from the dimensionless displacement (Δ) in the harmonic approximation by using the relation $\delta R = (\hbar/\mu\omega)^{1/2}\Delta$, where μ is the reduced mass (kg) and ω is the vibrational frequency (s^{-1}).

Assuming a wavenumber of 1662 cm^{-1} for the C═C stretch, a δR of 0.05 Å is obtained. This crude calculation assumes that the C═C stretch is localized in the 1662 cm^{-1} mode, that this is the only internal coordinate in this harmonic mode, and that the C atoms are not bound to anything else. Nevertheless, this bond length change compares favorably with the 0.14 Å increase predicted for the transition state. Interestingly, the resonance Raman spectra of thymine calculated previously from a Kramers−Kronig transform of the absorption spectrum and ab initio calculations of the ground- and excited-state structures of the nucleobases[18−20] could not accurately predict the intensity of the 1359 cm^{-1} band of thymine, suggesting that DFT methods combined with experimental measures of the ground- and excited-state dynamics may yield more accurate predictions of photochemical reaction mechanisms in thymine.

Recently, ultrafast time resolved infrared (IR) spectroscopy was used to determine the time scale of thymine dimerization.[38] The results show that marker bands for the photodimer were apparent within ~1 ps after excitation. The authors conclude that thymine dimerization is essentially barrierless in the excited state and ascribe the relatively low quantum yield for photodimer production to a paucity of ground-state structures with the correct orientation to form the photodimer within such a rapid time. This result is consistent with the preponderance of excited-state structural dynamics along the photochemical reaction coordinate reported here from the UV resonance Raman spectrum. Specifically, the possible formation of the transition-state structure, at least along the C_5═C_6 bond, within the period of the 1662 cm^{-1} mode (~20 fs) predicted here allows for several crossings of the transition state and subsequent vibrational relaxation within the ~1 ps formation time for the photodimer observed in the ultrafast IR spectrum. It is interesting to note the consistency between the structural dynamics measured here for the isolated thymine nucleobase in solution and the dynamics measured in the ultrafast IR spectra for $(dT)_{18}$, suggesting that the excited-state structural dynamics measured here for the nucleobases is relevant to DNA photochemistry.

It should be noted that the experimentally determined excited-state structural dynamics presented here are at odds with the CASSCF and DFT predictions of the excited-state potential energy surface along the photochemical reaction coordinate. These calculations of the excited-state potential energy surface of thymine along the photochemical reaction coordinate predict a shallow, almost flat, potential energy surface from the Franck−Condon region to the transition state, with a slight barrier just before reaching the transition state.[9,11,12] The resonance Raman intensity analysis presented here demonstrates that the initial excited-state potential energy slopes are nonzero and significant, particularly along the normal modes at 1662, 1359, and 1237 cm^{-1}. More recent SA-CASSCF calculations of uracil, an analogous pyrimidine nucleobase, with the double-ζ plus polarization Gaussian basis sets predict an excited-state potential energy surface with nonzero slopes at the Franck−Condon geometry along several normal modes.[39] This approach may provide a greater consistency with experimental results for thymine as well.

Excited-State Photophysics. The analysis presented here provides insight into the excited-state photophysics of thymine. Rigorous ab initio calculations on the electronic spectra and transition moments of thymine have reported that the lowest excited-state in solution is a $\pi\pi^*$ state.[40] The result presented here, namely, that thymine has an electronic transition moment of 3.5 D, supports the conclusion of this previous calculation; $\pi\pi^*$ states are expected to be symmetry allowed and have significant absorption oscillator strength and transition moment.

In the condensed phase, solvent dynamics may significantly contribute to the breadth of the absorption spectrum, either through inhomogeneous or homogeneous mechanisms. Homogeneous broadening in the condensed phase is normally dominated by solvent-induced dephasing, although population decay may also be important for thymine. To accurately model the magnitude of the resonance Raman cross-sections and the diffuseness of the absorption spectrum, it is necessary to include a Gaussian homogeneous line width of 355 cm^{-1} in thymine. The large homogeneous line width value for thymine represents the contributions from both population decay and dephasing. It is well-known that nonradiative processes, primarily internal conversion, are the primary population decay mechanism for the excited-state of thymine, with a quantum yield of $\sim10^{-4}$ for fluorescence and a nonradiative rate constant[2] of $\sim10^{-12}$ s^{-1}. Similarly low quantum yields for the formation of various photoproducts of thymine (0.018−0.007) indicate that internal conversion dominates the excited-state relaxation of their first excited state.[2] The exponential, first-order excited-state decay constant of thymine ($\sim10^{12}$ s^1) would yield a Lorentzian homogeneous line width in energy of ~5 cm^{-1}. However, the absorption spectrum and resonance Raman excitation profiles of thymine indicate that the homogeneous line width in energy is much larger and primarily Gaussian in shape. The exponential line shape can be converted to a Gaussian by assuming that the time integrals of both functions are identical. This yields a relation between Lorentzian and Gaussian line widths of $\Gamma_G = \Gamma_L(\pi/4)^{1/2}$ and a Gaussian line width of 3.5 cm^{-1}. This Gaussian population decay line width is insufficient to account for all of the homogeneous broadening necessary to reproduce the spectral diffuseness of the absorption spectrum and magnitude of the resonance Raman cross-sections of thymine. Thus, the primary contribution to the homogeneous line width is solvent-induced dephasing.

The inhomogeneous broadening arises from probing an ensemble of molecules, which have different solvation structures

leading to a distribution of electronic transition energies. The inhomogeneous broadening distribution is considered static on the resonance Raman time scale. Using DFT methods, Shishkin et al.[41] calculated the structures of uracil and thymine interacting with 11 water molecules and found significant differences in the interactions with the hydrophobic part of the nucleobases. In the case of uracil, the water molecules are located near the plane of the pyrimidine ring. The replacement of the hydrogen atom in uracil by the methyl group in thymine results in an extremely nonplanar arrangement of water molecules around the hydrophobic part of thymine due to steric crowding. Solvent-dependent frequency shifts and intensity changes have also been observed in the C═C stretch and other modes in the Raman spectra of thymine and thymidine as a function of solvent.[42] Because this double bond is the site of electronic excitation and the interaction of water molecules appears to be greater with the hydrophobic region in thymine than in uracil, this explanation would predict a high value of the inhomogeneous line width Θ for thymine, as observed. Since solvent-dependent dephasing is the primary homogeneous broadening mechanism, the greater interaction of solvent water molecules with the double bond in thymine may also account for the larger homogeneous line width for thymine. Clearly, it would be useful to measure the excited-state properties and line width values for uracil as a test of this model.

Conclusion

Self-consistent analysis of the resonance Raman spectra and absorption spectra is a powerful probe of excited-state structural dynamics. The results presented here clearly demonstrate that the excited-state structural dynamics of thymine are coincident with the expected photochemical reaction coordinate, leading toward the cyclobutyl dimer transition state. A comparison with the excited-state structural dynamics of uracil should be instructive in determining the factors that lead to different quantum yields for the different photoproducts in these two analogous pyrimidine nucleobases. These results are significant for developing a molecular mechanism of UV-induced nucleic acid damage, with its important physiological consequences and implications for the origins of life.

Acknowledgment. The authors thank NSERC Research Grants-in-Aid for funding this work. The authors also thank Prof. Anne Myers Kelley for providing the computer program for the time-dependent calculations.

References and Notes

(1) Lehninger, A. L. *Biochemistry*; Worth Publications: New York, 1975; Vol 2, pp 309−333.

(2) Ruzsicska, B. P.; Lemaire, D. G. E. In *CRC Handbook of Organic Photochemistry and Photobiology*; Horspool, W. H., Song, P.-S., Eds.; CRC Press: New York, 1995; pp 1289−1317.

(3) Brown, I. H.; Freeman, K. B.; Johns, H. E. *J. Mol. Biol.* **1966**, *15*, 640−662.

(4) (a) Greenstock, C. L.; Brown, I. H.; Hunt, J. W.; Johns, H. E. *Biochem. Biophys. Res. Commun*. **1967**, *27*, 431−436. (b) Burr, J. G.; Park, E. H. *Radiat. Res*. **1967**, *31*, 547−550.

(5) (a) Kang, H.; Taek Lee, K.; Jung, B.; Jae Ko, Y.; Keun Kim, S. *J. Am. Chem. Soc*. **2002**, *124*, 12958−12959. (b) He, Y.; Wu, C.; Kong, W. *J. Phys. Chem. A* **2003**, *107*, 5145−5148.

(6) Pecourt, J.-M. L.; Peon, J.; Kohler, B. *J. Am. Chem. Soc.* **2000**, *122*, 9348−9349.

(7) Onidas, D.; Markovitsi, D.; Marguet, S.; Sharonov, A.; Gustavsson, T. *J. Phys. Chem. B* **2002**, *106*, 11367−11374.

(8) Peon, J.; Zewail, A. H. *Chem. Phys. Lett.* **2001**, *348*, 255−262.

(9) Perun, S.; Sobolewski, A. L.; Domcke, W. *J. Phys. Chem. A* **2006**, *110*, 13238−13244.

(10) Zhang, R. B.; Eriksson, L. A. *J. Phys. Chem. B* **2006**, *110*, 7556−7562.

(11) Durbeej, B.; Eriksson, L. A. *Photochem. Photobiol*. **2003**, *78*, 159−167.

(12) Durbeej, B.; Eriksson, L. A. *J. Photochem. Photobiol., A* **2002**, *152*, 95−101.

(13) Wetmore, S. D.; Boyd, R. J.; Eriksson, L. A. *J. Phys. Chem. B* **1998**, *102*, 5369−5377.

(14) (a) Myers, A. B.; Mathies, R. A. In *Biological Applications of Raman Spectroscopy, Resonance Raman Spectra of Polyenes and Aromatics*; Spiro, T. G., Ed.; Wiley-Interscience: New York, 1987; Vol. 2, pp 1−58. (b) Myers, A. B. Excited electronic state properties from ground-state resonance Raman intensities. In *Laser Techniques in Chemistry*; Myers, A. B., Rizzo, T. R., Eds.; Wiley: New York, 1995; pp 325−384. (c) Kelley, A. M. *J. Phys. Chem. A* **1999**, *103*, 6891−6903.

(15) Fodor, A. P. A.; Rava, R. P.; Hays, T. R.; Spiro, T. G. *J. Am. Chem. Soc.* **1985**, *107*, 1520−1529.

(16) (a) Fodor, S. P. A.; Spiro, T. G. *J. Am. Chem. Soc.* **1986**, *108*, 3198−3205. (b) Perno, J. R.; Grygon, C. A.; Spiro, T. G. *J. Phys. Chem.* **1989**, *93*, 5672−5678.

(17) Kubasek, W. L.; Hudson, B.; Peticolas, W. L. *Proc. Natl. Acad. Sci. U.S.A.* **1985**, *82*, 2369−2373.

(18) Blazej, D.; Peticolas, W. L. *J. Chem. Phys.* **1980**, *72*, 3134−3142.

(19) Peticolas, W. L.; Blazej, D. C. *Chem. Phys. Lett.* **1979**, *63*, 604−608.

(20) (a) Chinsky, L.; Laigle, A.; Peticolas, W. L.; Turpin, P.-Y. *J. Chem. Phys.* **1982**, *76*, 1−5. (b) Peticolas, W. L.; Rush, T., III. *J. Comput. Chem.* **1995**, *16*, 1261−1270. (c) Rush, T., III; Peticolas, W. L. *J. Phys. Chem.* **1995**, *99*, 14647−14658.

(21) Webb, M. A.; Fraga, E.; Loppnow, G. R. *J. Phys. Chem.* **1996**, *100*, 3278−3287.

(22) Webb, M. A.; Kwong, C. M.; Loppnow, G. R. *J. Phys. Chem. B* **1997**, *101*, 5062−5069.

(23) Loppnow, G. R.; Fraga, E. *J. Am. Chem. Soc.* **1997**, *119*, 895−905.

(24) Mathies, R. A.; Oseroff, A. R.; Stryer, L. *Proc. Natl. Acad. Sci. U.S.A.* **1976**, *73*, 1−5.

(25) Fraga, E.; Loppnow, G. R. *J. Phys. Chem. B* **1998**, *102*, 7659−7665.

(26) Lee, S.-Y.; Heller, E. J. *J. Chem. Phys.* **1979**, *71*, 4777−4788.

(27) Mukamel, S. *Principles of Nonlinear Optical Spectroscopy*; Oxford University Press: New York, 1995.

(28) Li, B.; Johnson, A. E.; Mukamel, S.; Myers, A. B. *J. Am. Chem. Soc.* **1994**, *116*, 11039−11047.

(29) Shoute, L. C. T.; Loppnow, G. R. *J. Chem. Phys.* **2002**, *117*, 842−850.

(30) Szczepaniak, K.; Szczesniak, M. M.; Person, W. B. *J. Phys. Chem. A* **2000**, *104*, 3852−3863.

(31) Gaigeot, M.-P.; Leulliot, N.; Ghomi, M.; Jobic, H.; Coulombeau, C.; Bouloussa, O. *Chem. Phys.* **2000**, *261*, 217−237.

(32) Nishimura, Y.; Suboi, M.; Kato, S.; Morokuma, K. *J. Am. Chem. Soc.* **1981**, *103*, 1354−1358.

(33) Aida, M.; Kaneko, M.; Durpuis, M.; Ueda, T.; Ushizawa, K.; Ito, G.; Kumakura, A.; Tsuboi, M. *Spectrochim. Acta, Part A* **1997**, *53*, 393−407.

(34) (a) Barnes, A. J.; Stuckey, M. A.; Gall, L. L. *Spectrochim. Acta, Part A* **1984**, *40*, 419−431. (b) Toyama, A.; Takeuchi, H.; Harada, I. *J. Mol. Struct.* **1991**, *242*, 87−98. (c) Zhang, S. L.; Michaelian, K. H.; Loppnow, G. R. *J. Phys. Chem. A* **1998**, *102*, 461−470.

(35) Yarasi, S.; Billinghurst, B. E.; Loppnow, G. R. *J. Raman Spectrosc.* **2007**, in press.

(36) Marcus, R. A.; Sutin, N. *Biochim. Biophys. Acta* **1985**, *811*, 265−322.

(37) Kelley, A. M. *J. Phys. Chem. A* **1999**, *103*, 6891−6903.

(38) Schreier, W. J.; Schrader, T. E.; Koller, F. O.; Gilch, P.; Crespo-Hernandez, C. E.; Swaminathan, V. N.; Carell, T.; Zinth, W.; Kohler, B. *Science* **2007**, *315*, 625−629.

(39) Matsika, S. *J. Phys. Chem. A* **2004**, *108*, 7584−7590.

(40) Lorentzon, J.; Fülscher, M. P.; Roos, B. O. *J. Am. Chem. Soc.* **1995**, *117*, 9265−9273.

(41) (a) Shishkin, O. V.; Gorb, L.; Leszczynski, J. *Int. J. Mol. Sci.* **2000**, *1*, 17−27. (b) Shukla, M. K.; Leszczynski, J. *J. Phys. Chem. A* **2002**, *106*, 8642−8650. (c) Gaigot, M.-P.; Ghomi, M. *J. Phys. Chem. B* **2001**, *105*, 5007−5017.

(42) Beyere, L.; Arboleda, P.; Monga, V.; Loppnow, G. R. *Can. J. Chem.* **2004**, *82*, 1092−1101.